

Diffusion Behaviours of Three Thioureido Imidazoline Corrosion Inhibitors in a Simulated Sediment Layer

Zhiwei Tie¹, Wenwen Song², Jingmao Zhao^{1,3,*}

¹ College of Material Science and Engineering, Beijing University of Chemical Technology, Beijing 100029, China

² Research Institute of Oil-gas Engineering, Tarim Oilfield Company, Petrochina, Korla 841000, China

³ Beijing Key Laboratory of Electrochemical Process and Technology for Materials, Beijing 100029, China

*E-mail: jingmaozhao@126.com

Received: 10 February 2018 / Accepted: 11 April 2018 / Published: 10 May 2018

In the present work, the diffusion behaviours of three thioureido imidazoline inhibitors (SOIMS, SOIM and OIM) in a simulated sediment layer were investigated by ultraviolet-visible spectrophotometry (UV-vis) and potentiodynamic polarization in a simulation setup. The simulated sediment layer was characterized by SEM and mercury intrusion experiments. SEM observation shows that the sediment layer obtained in this experiment is relatively dense with no large pores. The mercury intrusion experiment was used to analyse the pore size distribution of the simulated deposition. UV-vis experiments show that the diffusion behaviours of corrosion inhibitors are related to their water solubility. The better the water solubility of the corrosion inhibitors, the stronger their ability to diffuse through the sediment layer. The UV-vis and potentiodynamic polarization results suggest that the three corrosion inhibitors can diffuse through the sediment layer as the diffusion time increases.

Keywords: Corrosion inhibitor; Diffusion; Sediment layer; Carbon steel; Potentiodynamic polarization

1. INTRODUCTION

Corrosion under sediment or under deposit corrosion (UDC) [1-3] is frequently encountered in oil/gas production, transportation and processing, which can cause serious local corrosion due to uneven sediment coverage on steel surface.

Zhu *et al.* [4] studied the corrosion behaviours of ammonium chloride sediment on top of a reactor effluent air cooler (REAC) and found that the sediment unevenly thinned the top of the reactor

tube and caused severe local corrosion. Wang *et al.* [5] investigated the corrosion behaviours of mixed sediments on carbon steel in seawater and revealed severe local corrosion of carbon steel under mixed sediments.

Corrosion inhibitor additives can effectively inhibit the inner surface corrosion of carbon steels and equipment, and have been widely used in oil and gas exploitation and transportation. However, carbon steel surfaces are usually covered by a layer of sediment, which hinders the adsorption of corrosion inhibitors on the surfaces. Therefore, the diffusion of corrosion inhibitors through the sediment layer on a steel surface to inhibit corrosion under the sediment has become a hot research topic. Zhu *et al.* [6] investigated the inhibition effects of $C_{12}H_{23}O_2^-$ on the corrosion of N80 steel under sediment in a neutral NaCl solution in an occluded cell that was used to simulate local corrosion processes and found that $C_{12}H_{23}O_2^-$ could adsorb on the N80 steel surface and effectively inhibit its corrosion. Tan *et al.* [7] studied under-sediment corrosion behaviours using a wire beam electrode and found that the sediment deposited area in a CO_2 solution was in the cathode state, and caused local corrosion only in the presence of O_2 or with added corrosion inhibitor. In addition, the overall corrosion rate decreased and the local corrosion became more severe with the increasing corrosion inhibitor concentration. Pedersen *et al.* [8] investigated galvanic corrosion between the sand-covered and bare carbon steel specimens in two cases, e.g. covering the steel specimen with sand before and after the corrosion inhibitor was added. Their results suggested that a certain concentration of corrosion inhibitor could reduce the galvanic current between the steel specimens, but in both cases, obvious local corrosion was found on the sand-covered carbon steel specimens. In addition, the steel covered with sand first exhibited more severe local corrosion, possibly because the sand layer on the steel surface absorbed a certain amount of the corrosion inhibitor and blocked the mass transfer of the corrosion inhibitor to the carbon steel specimen surface. Therefore, a higher concentration of inhibitors was required to inhibit such corrosion.

A corrosion inhibitor can only inhibit metal corrosion if it penetrates the sediment layer and reaches the metal matrix. The studies mentioned above demonstrated that corrosion inhibitors could penetrate sediments by indirect means, but lacked direct evidence. In addition, no diffusion rules for corrosion inhibitors in sediments have been reported. In the present work, the diffusion behaviours of three thioureido imidazoline corrosion inhibitors in sediments were studied using a simple simulation setup by SEM, mercury intrusion experiment, ultraviolet-visible spectrophotometry (UV-vis), and potentiodynamic polarization measurement.

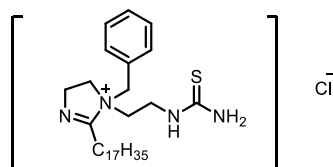
2. MATERIALS AND METHODS

2.1. Preparation of the sediment layer, solutions and corrosion inhibitor

White cement (main ingredient of $CaSiO_3$, which is commercially available), $MgCO_3$, $CaSO_4$ and water were mixed in a mass ratio of 10:3:3:8 and pressed into round discs with a diameter of 30 mm and a thickness of 3 mm. These samples were kept at 25 °C for 8 h, incubated in a 40 °C oven for 24 h and then as the simulated sediment layer. A 3.5 wt% NaCl solution was prepared with analytical

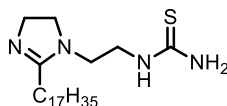
grade reagents and deionized water, and used as the test solution. Fig. 1 shows the molecular structures of the three thioureido imidazoline corrosion inhibitors used in this experiment. Thioureido imidazoline can strongly adsorb on steel surfaces because of its strongly electronegative unsaturated double bonds of S and N, and has been reported to effectively inhibit metal corrosion in a CO₂ environment [9-11]. Among them, OIM (oleic acid imidazoline) is an oil-soluble corrosion inhibitor, SOIMS (thiourea oleic acid imidazoline quaternary ammonium salt) is a water-soluble corrosion inhibitor, and the water-solubility of SOIM (thiourea oleic acid imidazoline) falls somewhere in between the other two compounds.

SOIMS:



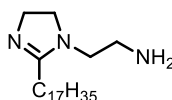
1-benzyl-2-heptadecyl-1-(2-thioureidoethyl)-4,5-dihydro-1H-imidazol-1-ium chloride

SOIM:



1-(2-(2-heptadecyl-4,5-dihydro-1H-imidazol-1-yl)ethyl)thiourea

OIM:



2-(2-heptadecyl-4,5-dihydro-1H-imidazol-1-yl)ethanamine

Figure 1. Molecular structures of (a) OIM, (b) SOIM and (c) SOIMS used in the experiment

2.2. Simulation setup

The experimental apparatus shown in Fig. 2 was used to study the diffusion of the corrosion inhibitors through the simulated sediment layer. The setup consisted of two containers of 600 mL, which both contained 500 mL of 3.5 wt% NaCl solution. The corrosion inhibitor was added at a concentration of 200 mg/L to the left container. The containers were connected to allow the corrosion inhibitor to diffuse from the left container through the sediment layer in the middle to the right container. The concentration of the corrosion inhibitor in the right container was measured at pre-set time intervals.

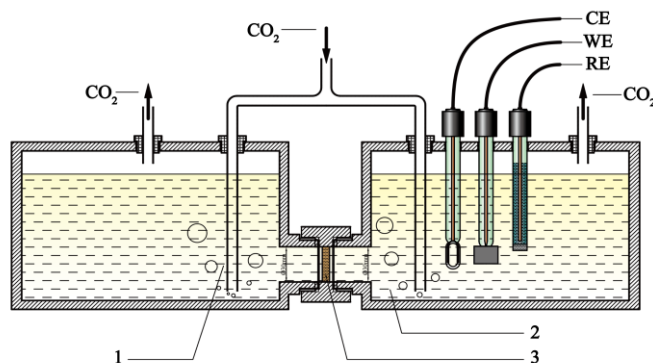


Figure 2. Simulation setup for studying corrosion inhibitor diffusion through sediment layers on a steel surface.

2.3. UV-Vis spectrophotometry

2.3.1 Determination of the maximum absorption wavelength and standard curve of the corrosion inhibitor

The imidazoline molecule contains a C=N double bond that usually results in a maximum absorption at 200-300 nm [12]. The maximum absorption wavelength can be determined by recording the variation in the absorbance with wavelength. According to the Beer-Lambert law [13], the absorption of a substance is directly proportional to its concentration, which can be used to quantitatively analyse the concentration of the compound. In the present work, the UV-Vis absorption of the corrosion inhibitor was measured using a UV1700pc UV-Vis spectrophotometry with 0.2 g/L cresol red as the chromogenic agent and 3 mol/L phosphoric acid as the buffer solution. The corrosion inhibitor was dissolved in 3.5 wt% NaCl to prepare a 100 mg/L stock solution. Aliquots of 0, 1, 2, 3, 4, 5 and 6 mL of the stock solution were respectively added to 1 cm cuvettes, mixed with 0.1 mL of chromogenic agent and 0.5 mL buffer, brought to 10 mL with a 3.5wt% NaCl solution, shake, allowed to develop at 25 °C for 0.5 h, and measured for their UV-Vis absorption using a UV1700pc UV-Vis spectrophotometry in the wavelength range of 200-400 nm. A solution without the corrosion inhibitor was used as the blank. A standard curve was established at the maximum absorption wavelength.

2.3.2 Determination of the corrosion inhibitor concentration

Two 10 mL tubes (#1 and #2) contained 0.1 mL of the chromogenic agent and 0.5 mL of the buffer solution, respectively. The volume of tube #1 was brought to 10 mL with 3.5 wt% NaCl and used as the reference solution. The testing solution was added to tube #2 to bring the volume to 10 mL. The tube was shaken well and allowed to develop at 25 °C for 30 min, and then the UV-vis absorption was measured in the wavelength range of 200-400nm using a 1 cm cuvette on the UV1700pc UV-Vis spectrophotometry using the solution in tube #1 as the reference. The concentration of the corrosion inhibitor was obtained by fitting the standard curve to the absorbance at the maximum absorption

wavelength. The corrosion inhibitor concentration of the solution in the right container of the experimental apparatus was measured daily for 15 days. The experimental temperature was 25 °C.

2.4. Potentiodynamic polarization measurements

Potentiodynamic polarization measurements were conducted in the right container of the experimental apparatus every 3 days to evaluate the diffusion and inhibition effect of the corrosion inhibitor. The potentiodynamic polarization curves were measured using a CS350 electrochemical workstation consisting of a classical three-electrode system with a platinum electrode as the counter electrode and a saturated calomel electrode as the reference electrode. A Q235 steel electrode was polished, cleaned, sealed with an epoxy resin, and used as the working electrode. The surface area of the working electrode area was 1 cm². The chemical composition of the Q235 carbon steel used in the present work was 0.17 wt.% C, 0.20 wt.% Si, 0.45 wt.% Mn, 0.01 wt.% P, 0.03 wt.% S, and bal. Fe.

The potentiodynamic polarization curves were measured in the potential range from -200 mV to +200 mV vs the open circuit potential (OCP) at a scanning rate of 0.5 mV/s and the curve data were fitted with the CS350 workstation software. The obtained corrosion current density (i_{corr}) was used to calculate the corrosion inhibition efficiency (η_p) of the corrosion inhibitor using eq. (1).

$$\eta_p = \frac{i_{corr} - i_{corr(inh)}}{i_{corr}} \times 100\% \quad (1)$$

where i_{corr} and $i_{corr(inh)}$ are the corrosion current densities before and after the corrosion inhibitor is added, respectively.

2.5. Characterization of the sediment layer

SEM (FEI Quanta 200F) was used to observe the surface topography of the sediment layer. Mercury intrusion experiments were performed using an AutoPore IV 9500 instrument to measure the pore size distribution of the sediment layer.

3. RESULTS AND DISCUSSION

3.1. UV-Vis spectroscopic analysis

3.1.1 Standard curve of the corrosion inhibitor

Fig. 3(a) shows the UV-Vis absorption curves of the different concentrations of the SOIMS corrosion inhibitor. The maximum absorption was 235 nm, which is consistent with the maximum absorption of imidazoline in the UV region at 230 nm reported in the literature [14,15]. Therefore, the absorbance of the corrosion inhibitor at 235 nm was plotted vs its concentration to establish the standard curve shown in Fig. 3(b). Clearly, the absorption of the corrosion inhibitor at 235 nm linearly increased with its concentration in the testing range with a linear equation of $A=0.0116C-0.0305$,

where A is the absorbance and C is the mass concentration of the corrosion inhibitor in mg/L. The Pearson's correlation coefficient was 0.9994, which indicated the good linearity of the standard curve. Fig. 4(a) shows the UV-Vis absorption curves of the different concentrations of the SOIM corrosion inhibitor. The absorbance of the corrosion inhibitor at 235 nm was plotted vs its concentration to establish the standard curve shown in Fig. 4(b). The curve shows that the absorption of the corrosion inhibitor at 235 nm linearly increased with its concentration in the testing range with the linear equation of $A=0.0268C-0.0736$, where A is the absorbance and C is the mass concentration of the corrosion inhibitor in $\text{mg}\cdot\text{L}^{-1}$. The Pearson's correlation coefficient was 0.9998, which indicated that the linearity of the standard curve was very good. The UV-Vis absorption curves of the different concentrations of the OIM corrosion inhibitor are shown in Fig. 5(a). The absorbance of the OIM corrosion inhibitor at 232 nm was plotted vs. its concentration to establish the standard curve shown in Fig. 5(b). This curve demonstrates that the absorption of the corrosion inhibitor at 232 nm is linearly increased with its concentration in the testing range with a linear equation of $A=0.0170C-0.0400$, where A is the absorbance and C is the mass concentration of the corrosion inhibitor in mg/L. The Pearson's correlation coefficient was 0.9932, which indicated that the linearity of the standard curve was good.

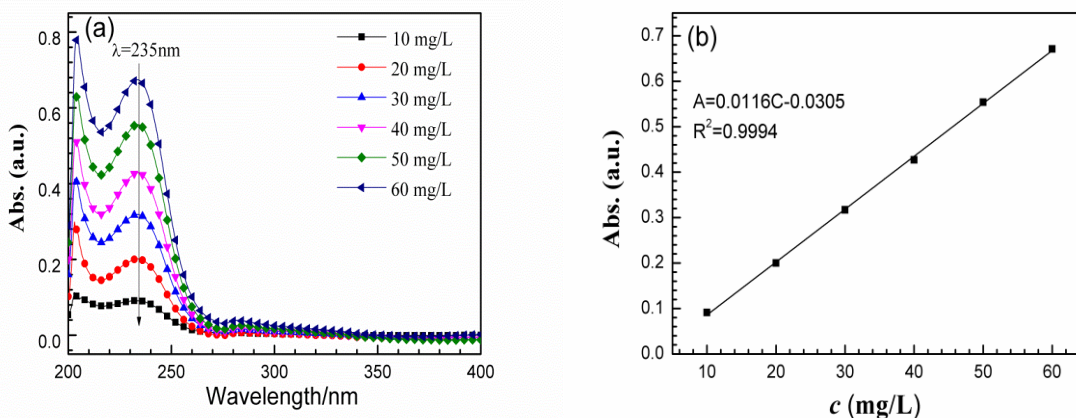


Figure 3. (a) UV-vis absorption spectra of the SOIMS corrosion inhibitor at different concentrations and (b) the standard curve of the corrosion inhibitor

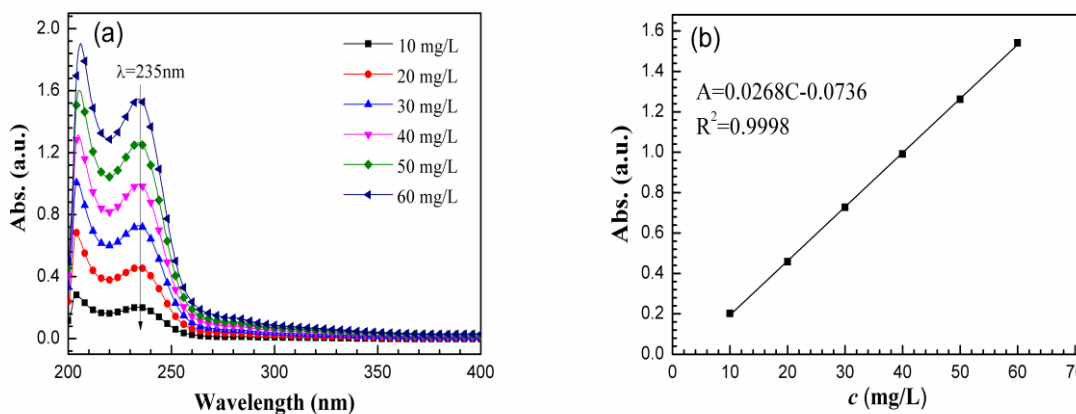


Figure 4. (a) UV-vis absorption spectra of the SOIM corrosion inhibitor at different concentrations and (b) the standard curve of the corrosion inhibitor

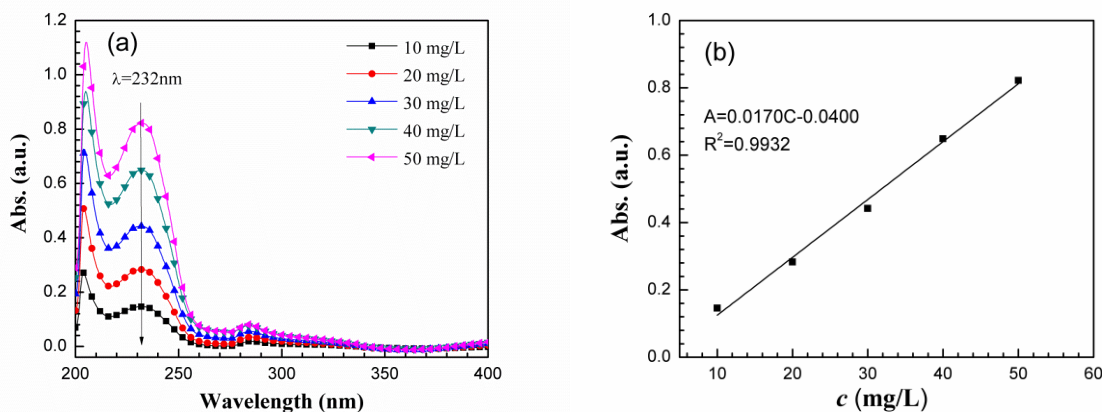


Figure 5. (a) UV-vis absorption spectra of the OIM corrosion inhibitor at different concentrations and (b) the standard curve of the corrosion inhibitor

3.1.2 Determination of the corrosion inhibitor concentration

Fig. 6(a) shows the UV-Vis absorption spectra of the solution in the right container of the experimental setup measured at different immersed time after adding the SOIMS corrosion inhibitor. The characteristic absorption peak of the corrosion inhibitor at 235 nm appeared after 1 day and the absorption increased as the diffusion time increased, which indicated that the corrosion inhibitor was able to diffuse through the sediment layer. The variation in the concentration and absorbance of the SOIMS corrosion inhibitor in the right container over time are shown in Fig. 6(b). It is clear that the corrosion inhibitor amount that passed through the sediment layer increased as the test time increased. The diffusion process shown in Fig. 6(b) can be divided into two stages. The first stage at day 1-11 is defined as the rapid diffusion stage. After 1 day, the corrosion inhibitor, SOIMS, starts to diffuse through the sediment layer, and an equivalent of 3.4% of the corrosion inhibitor (6.75 mg/L / 200 mg/L) reached the right container. Over time, the SOIMS corrosion inhibitor diffused more rapidly through the sediment layer. After 11 days, the concentration in the right container reached 32.63 mg/L, which is equivalent to 16.3% (32.63 mg/L / 200 mg/L) of the corrosion inhibitor passing through the sediment layer. The corrosion inhibitor, SOIMS, is a water-soluble corrosion inhibitor; its dissolution in solution is very good. It can quickly reach the right container through the sediment layer and is driven by the concentration difference. The second stage at day 11-15 is defined as the late diffusion stage, and the diffusion of the corrosion inhibitor through the sediment layer was slow. This might be explained by the corrosion inhibitor concentration in the left container decreasing and that in the right container increasing as the diffusion time increases, leading to a smaller concentration difference. The concentration difference is the driving force of the diffusion. Therefore, the diffusion rate of the corrosion inhibitor through the sediment layer decreases as the diffusion time prolonged. The corrosion inhibitor concentration in the right container reaches 37.36 mg/L at day 15, which is equivalent to 18.7% (37.36 mg/L / 200 mg/L) of the corrosion inhibitor diffusing through the sediment layer.

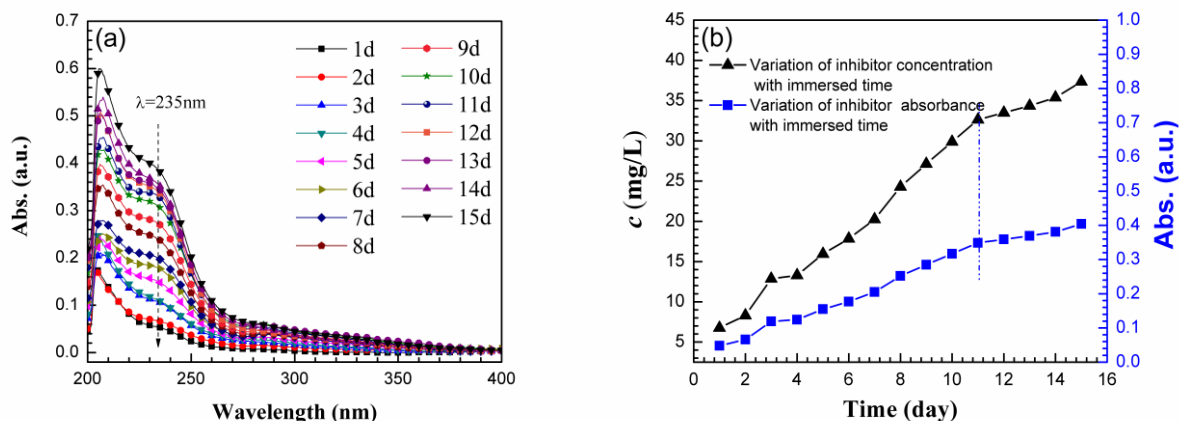


Figure 6. (a) UV-Vis absorption spectra of the solution in the right container of the experimental device at different immersed time after adding SOIMS inhibitor and (b) variation in the inhibitor concentration and absorbance over the immersed time

Fig. 7(a) shows the UV-Vis absorption spectra of the solution in right container of the experimental setup measured at different immersed time after adding the SOIM corrosion inhibitor. The characteristic absorption peak of the corrosion inhibitor at 235 nm appears after 1 day and the absorption increases with the prolongation of the diffusion time, indicating that this inhibitor can also diffuse through the sediment layer. The variation in the concentration and absorbance of the corrosion inhibitor in the right container over time are shown in Fig. 7(b). The corrosion inhibitor amount that passed through the sediment layer increased with the prolonged test time. The diffusion process shown in Fig. 7(b) can be divided into three stages. The first stage at day 1-5 is defined as the early diffusion stage, and the corrosion inhibitor concentration increased from 0 to 12 mg/L, which is equivalent to 6% (12 mg/L / 200 mg/L) of the corrosion inhibitor penetrating the sediment layer, in 5 days. During this stage, the diffusion rate of the corrosion inhibitor in the sediment layer is relatively low due to the dense sediment layer with small pores. The corrosion inhibitor requires a longer time to diffuse through the sediment layer. The water solubility of SOIM is not as high as that of SOIMS. The slow diffusion behaviour at this stage is related to its water solubility. During the second stage of day 5-11, which is defined as the rapid diffusion stage, the corrosion inhibitor rapidly passes through the sediment layer and its concentration in the right container reaches 37 mg/L, which is equivalent to 18.5% (37 mg/L / 200 mg/L) of the corrosion inhibitor passing through the sediment layer, at the end of the stage. The third stage at day 11-15 is defined as the late diffusion stage where the diffusion of the corrosion inhibitor in the sediment layer becomes slow again. This might be explained by the corrosion inhibitor concentration in the left container decreasing and that in the right container increasing as the diffusion time increases, leading to a smaller concentration difference. The concentration difference is the driving force of the diffusion. Therefore, the diffusion rate of the corrosion inhibitor through the sediment layer becomes lower as the diffusion time is prolonged. The corrosion inhibitor concentration in the right container reaches 45 mg/L at day 15, which is equivalent to 22.5% (45 mg/L / 200 mg/L) of the corrosion inhibitor diffusing through the sediment layer. These results are consistent with the results of Nahali[16] on the effects of Na_3PO_4 on the diffusion

behaviours of Cl^- in mortar, and the diffusion process of Cl^- in the mortar was also divided into three stages.

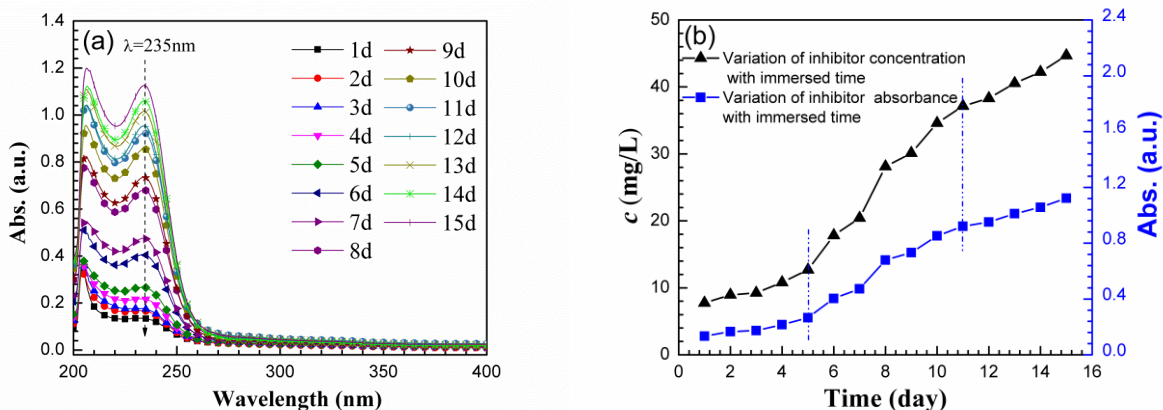


Figure 7. (a) UV-Vis absorption spectra of the solution in the right container of the experimental device at different immersed time after adding the SOIM inhibitor and (b) variation in the inhibitor concentration and absorbance with immersed time

Fig. 8(a) shows the UV-vis absorption spectra of the solution in the right container of the experimental setup measured at different immersed time after adding the OIM corrosion inhibitor. The characteristic absorption peak of the OIM corrosion inhibitor at 232 nm is not obvious in the first 10 days, which indicated that the amount of the OIM corrosion inhibitor that passed through the sediment layer was very small. After 10 days, the characteristic absorption peak of the OIM corrosion inhibitor increased significantly. The variation in the concentration and absorbance of the OIM corrosion inhibitor in the right container with time are shown in Fig. 8(b). The diffusion process shown in Fig. 8(b) can be divided into two stages. The first stage at day 1-10 is defined as the early diffusion stage. The concentrations of the OIM corrosion inhibitor detected in the first 10 days were very low and essentially unchanged. At the end of this period, 4.29 mg/L of the corrosion inhibitor was detected in the right container, which is equivalent to 2.1% ($4.29 \text{ mg/L} / 200 \text{ mg/L}$) of the inhibitor diffusing through the sediment layer to the right container. The diffusion rate of the OIM corrosion inhibitor at this stage is relatively slow. The OIM inhibitor is an oil-soluble corrosion inhibitor. The slow diffusion rate of the corrosion inhibitor at this stage may be related to the water solubility of this corrosion inhibitor. The second stage is 10-15 d, and during this time, the diffusion rate of the corrosion inhibitor through the sediment accelerated significantly. At the end of this period, the right solution contained 8.29 mg/L of corrosion inhibitor, which is equivalent to 4.1% ($8.29 \text{ mg/L} / 200 \text{ mg/L}$) of the corrosion inhibitor diffusing through the sediment layer to the right solution. Overall, this inhibitor has a very poor diffusion behaviour in the sediment layer.

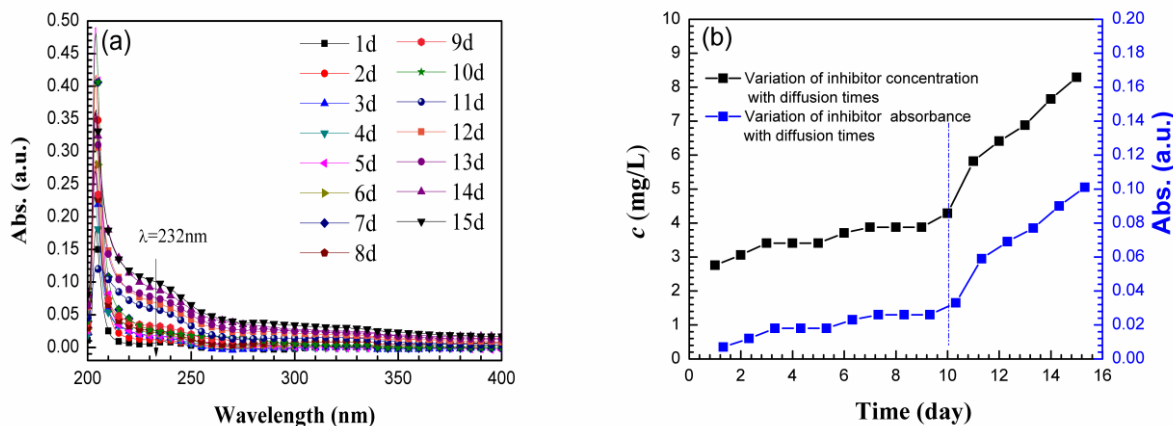


Figure 8. (a) UV-Vis absorption spectra of the solution in the right container of the experimental device at different immersed time after adding the OIM inhibitor and (b) variation in the inhibitor concentration and absorbance over immersed time

3.2. Electrochemical measurements

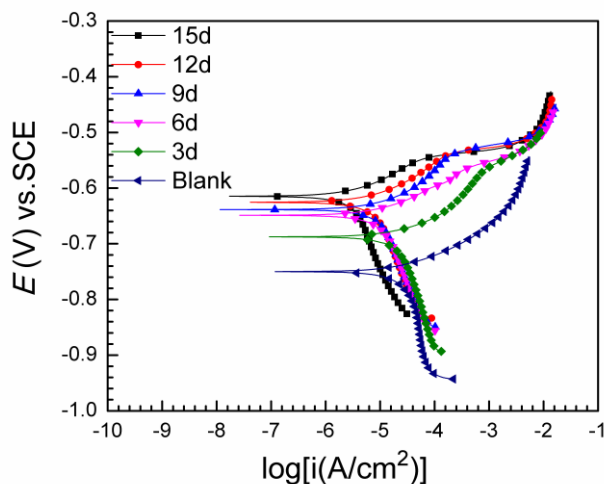


Figure 9. The polarization curves of Q235 steel at different immersed time after adding the SOIMS inhibitor

Potentiodynamic polarization measurements were obtained every 3 days in the right container. Fig. 9 shows the polarization curves for the diffusion process of the SOIMS corrosion inhibitor. The corrosion potential gradually increased with the prolongation of the diffusion time, which indicated that the corrosion inhibitor is an anodic corrosion inhibitor [17]. The fitting data of the polarization curves are shown in Table 1. The decrease in the corrosion current density of the carbon steel with the diffusion time of corrosion inhibitor suggests that the SOIMS corrosion inhibitor can penetrate the sediment layer to protect the carbon steel surface. The polarization curves for the diffusion process of the SOIM corrosion inhibitor are shown in Fig. 10. Table 2 shows the fitting data of the polarization curves. As the diffusion time increases, the corrosion current density gradually decreases, demonstrating that the SOIM corrosion inhibitor could diffuse through the sediment layer to protect

the carbon steel as well. Fig. 11 shows the polarization curves in the diffusion process of OIM corrosion inhibitor and the fitting data are shown in Table 3. Since OIM corrosion inhibitor diffuses through the sediment layer at a lower rate, the corrosion inhibition efficiency is relatively lower than that of SOIMS and SOIM.

Table 1. Electrochemical parameters of Q235 steel in solution at different immersed time after adding the SOIMS corrosion inhibitor

Time (d)	E_{corr} vs. SCE (mV)	β_a (mV/dec)	β_c (mV/dec)	i_{corr} ($\mu\text{A}/\text{cm}^2$)	Corrosion rate (mm/a)	η_p (%)
0	-748	45.4	-296.9	27.9	0.3269	-----
3	-686	47.1	-241.3	22.6	0.2649	18.97
6	-649	47.6	-228.9	10.7	0.1259	61.49
9	-639	51.1	-172.5	10.0	0.1175	64.06
12	-625	52.2	-161.1	7.7	0.0898	72.53
15	-616	49.2	-197.7	3.6	0.0424	87.03

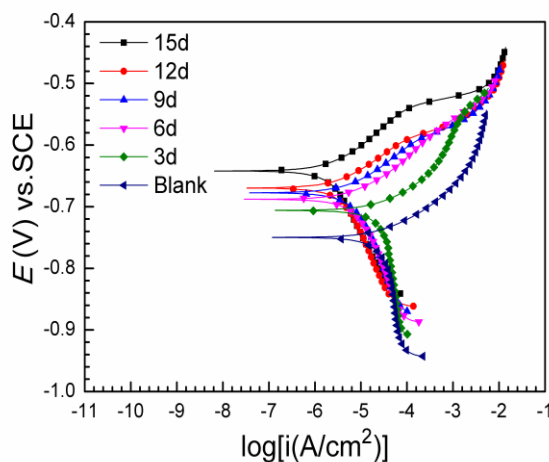


Figure 10. The polarization curves of Q235 steel at different immersed time after adding the SOIM inhibitor

Table 2. Electrochemical parameters of Q235 steel in solution at different immersed time after adding the SOIM corrosion inhibitor

Time (d)	E_{corr} vs. SCE (mV)	β_a (mV/dec)	β_c (mV/dec)	i_{corr} ($\mu\text{A}/\text{cm}^2$)	Corrosion rate (mm/a)	η_p (%)
0	-748	45.4	-296.9	27.9	0.3269	-----
3	-705	47.6	-228.8	25.5	0.2996	8.35
6	-688	54.4	-143.1	6.8	0.0795	75.68
9	-676	56.4	-130.6	5.6	0.0658	79.87
12	-669	54.3	-143.4	3.5	0.0415	87.30
15	-645	55.3	-136.8	2.3	0.0264	91.92

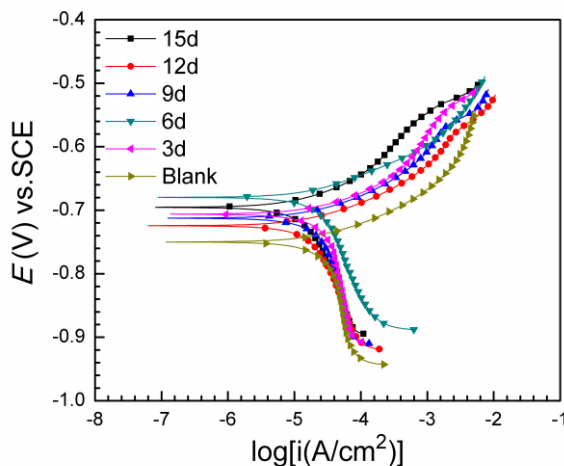


Figure 11. The polarization curves of Q235 steel at different immersed time after adding the OIM inhibitor

Table 3. Electrochemical parameters of Q235 steel in solution at different immersed time after adding the OIM corrosion inhibitor

Time (d)	E_{corr} vs. SCE (mV)	β_a (mV/dec)	β_c (mV/dec)	i_{corr} ($\mu\text{A}/\text{cm}^2$)	Corrosion rate (mm/a)	η_p (%)
0	-748	45.4	-296.9	27.9	0.3269	-----
3	-708	47.5	-230.8	24.6	0.2875	12.05
6	-680	47.8	-224.4	22.9	0.2684	17.90
9	-712	46.5	-257.8	21.9	0.2565	21.54
12	-724	45.4	-298.9	18.3	0.2149	34.26
15	-695	49.8	-187.7	13.0	0.1523	53.41

3.3. SEM analysis

Fig.12. A and B show the SEM images of the sediment surface before and after 15 days of diffusion of the SOIM corrosion inhibitor, respectively. It can be seen from the microscopic morphology of the sedimentary layer that the sediment layer obtained in this experiment is relatively dense with no large pores. Therefore, the layer can be used as a simulated sediment layer to study the diffusion of corrosion inhibitors.

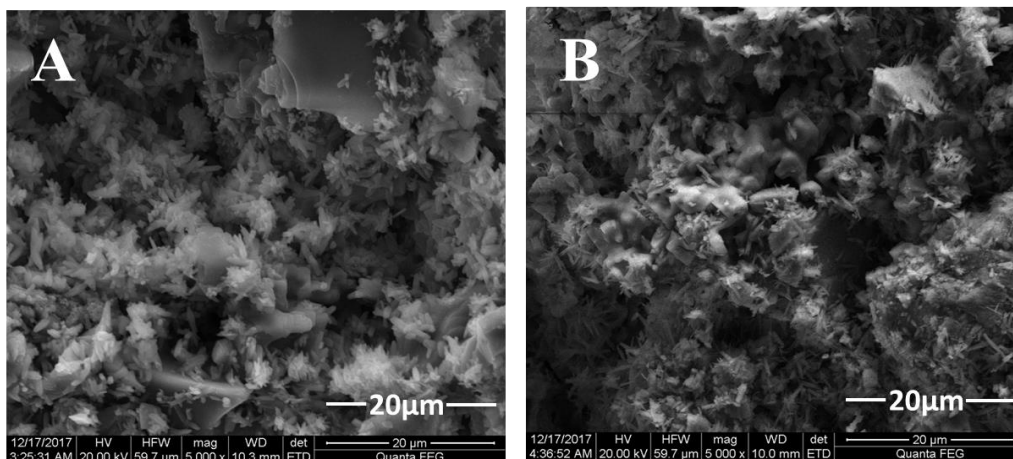


Figure 12. SEM micrograph of the sediment surface before (A) and after (B) 15 days of diffusion of the SOIM corrosion inhibitor

3.4. Mercury intrusion analysis

To analyse the pore size distribution of the simulated deposition, we conducted mercury intrusion experiment [18,19]. Fig.13 (a) shows the pore size distribution of the simulated deposition before the experiment. We determined that get the pore size is distributed in the range of 7~20 microns. And Fig.13 (b) shows the pore size distribution of the simulated deposition after a 15 day diffusion test with the SOIM corrosion inhibitor. The pore size is in the range of 7~100 microns. This result demonstrates that the pore size of the sediment layer increases after 15 days of immersion and infiltration of the SOIM corrosion inhibitors.

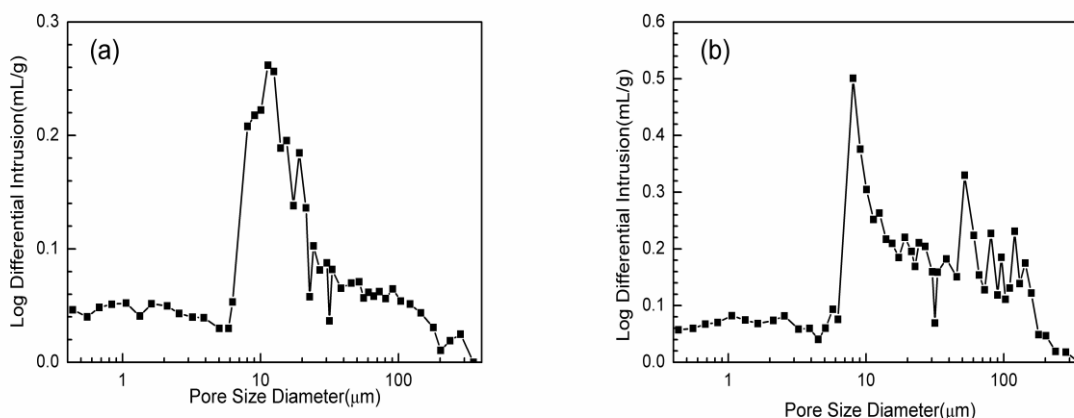


Figure 13. The pore size distribution of the simulated deposition before (a) and after (b) 15 days of diffusion of the SOIM corrosion inhibitor

3.5. Discussion

Adding corrosion inhibitors is an effective and common method to inhibit corrosion under sediment. A corrosion inhibitor can only inhibit metal corrosion well if it passes through the sediment

layer and reaches the metal matrix. There are many indirect ways to study the inhibition performance of corrosion inhibitors against UDC [6-8], yet there is a lack of direct evidence. In the experiment, we designed a simple and practical simulated setup to directly research the diffusion behaviour of corrosion inhibitors. Previous research showed that a corrosion inhibitor could reach a steel surface without being depleted after a sufficient amount is added [8,20]. In this study, the corrosion inhibitor concentration of 200 mg/L was added to the solution. The UV-vis spectrophotometry method indicated that the three corrosion inhibitors could pass through the sediment layer over the prolonged test time. The results of the potentiodynamic polarization demonstrated that the three corrosion inhibitors were able to diffuse through the sediment layer to inhibit the corrosion of carbon steels.

It is crucial to select a specific corrosion inhibitor to inhibit corrosion under sediment. The structure of the corrosion inhibitor molecule affects its corrosion inhibition mechanism and performance to some extent [21,22]. Different corrosion inhibitors have different water solubilities and adsorption properties. The poor water solubility of a corrosion inhibitor impedes its application. The introduction of foreign groups affects their water solubility and inhibition efficiency [23,24]. In this experiment, OIM is an oil-soluble corrosion inhibitor, SOIMS is a water-soluble corrosion inhibitor, and the solubility of SOIM falls somewhere in between the other two. From Fig. 6, 7 and 8, we can see that the three corrosion inhibitors can pass through the sediment layer over the test time. However, their diffusion rates are different. Both SOIMS and SOIM have a significantly faster diffusion rate than OIM. By comparing Fig. 6 (b) with Fig. 7 (b), we find that the diffusion rate of SOIMS is faster than that of SOIM. The concentration of SOIMS that diffused through the sediment layer gradually increased on days 1-11. However, the concentration of SOIM that diffused through the sediment layer slowly increased, and the diffusion rate of the corrosion inhibitor in the sediment layer was relatively low on days 1-5. This is related to the water solubility of the two corrosion inhibitors. The water solubility of an imidazoline corrosion inhibitor can be greatly enhanced by quaternization [25]. SOIMS can be synthesized via the quaternization of SOIM, and the water solubility of SOIMS is greater than that of SOIM. SOIMS and SOIM contain S atoms, which can strongly adsorb on a metal matrix [9-11]. Therefore, the inhibition efficiencies of both SOIMS and SOIM are obviously better than that of OIM from the potentiodynamic polarization analyses. It can be seen from the SEM results that the sediment layer obtained in this experiment is relatively dense with no large pores. Therefore, the layer can be used as a simulated sediment layer to study the diffusion of corrosion inhibitors. The mercury intrusion analysis demonstrates that the pore size of the sediment layer becomes larger after 15 days of immersion.

The experiment is a direct means to research the diffusion behaviours of corrosion inhibitors in a simulated sediment layer. We determined the diffusion behaviour of imidazoline corrosion inhibitors in a sediment layer. The results show that the diffusion behaviours of corrosion inhibitors are related to their water solubility. The higher the water solubility of a corrosion inhibitor, the stronger its ability to diffuse through the sediment layer. Perhaps the diffusion behaviours of inhibitors are related to other factors, such as the temperature and concentration. These details will be studied in our future work.

4. CONCLUSIONS

In the present work, the diffusion behaviours of three imidazoline inhibitors in a simulated sediment layer were investigated by SEM, mercury intrusion experiments, UV-vis spectrophotometry, and potentiodynamic polarization measurements. A simple and practical experimental setup was designed to simulate the diffusion of corrosion inhibitors through a sediment layer. The SOIMS corrosion inhibitor exhibits a maximum absorption at 235 nm, and its absorption was linearly related to its concentration in the test range with a Pearson's correlation coefficient of 0.9994. The SOIM corrosion inhibitor exhibits a maximum absorption at 235 nm, and its absorption was linearly related to its concentration in the test range with the Pearson's correlation coefficient of 0.9998. The OIM corrosion inhibitor exhibits a maximum absorption at 232 nm, and its absorption was linearly related to its concentration in the test range with a Pearson's correlation coefficient of 0.9932. The diffusion behaviours of a corrosion inhibitor are related to their water solubility. The results demonstrate that a better water solubility of a corrosion inhibitor, results in a stronger ability to diffuse through the sediment layer. The diffusion ability from strong to weak has the following relationship: SOIMS > SOIM > OIM. The results of the potentiodynamic polarization experiments demonstrate that the three corrosion inhibitors can diffuse through the sediment layer to inhibit the corrosion of carbon steels by day 15.

ACKNOWLEDGEMENT

The authors thank the National Natural Science Foundation of China for financial support for this project (No. 51471021).

References

1. Z. J. Zheng, G. F. Ou, H. J. Ye, J. L. Tan and H. Z. Jin, *Eng. Fail. Anal.*, 79 (2017) 726.
2. H. H. Almahamedh, *Procedia Eng.*, 114 (2015) 34.
3. Y. Bu, L. Wang, X. Chen, X. Wei, L. Deng and D. Che, *Appl. Therm. Eng.*, 131 (2018) 669.
4. M. Zhu, G. F. Ou, H. Z. Jin, K. X. Wang and Z. J. Zheng, *Eng. Fail. Anal.*, 57 (2015) 483.
5. X. Wang and R. E. Melchers, *J. Loss. Prevent. Proc.*, 45 (2017) 29.
6. Y. L. Zhu, X. P. Guo and Y. B. Qiu, *Corros. Eng. Sci. Techn.*, 45 (2010) 442.
7. Y. J. Tan, Y. F. Wu and K. Bhardwaj, *Corros. Sci.*, 53 (2011) 1254.
8. A. Pedersen, K. Bilkova, E. Gulbrandsen and J. Kvarekval, CO₂ corrosion inhibitor performance in the presence of solids: test method development, Corrosion 2008, New Orleans, Louisiana, America, 2008, paper No. 632.
9. G. A. Zhang, C. F. Chen, M. X. Lu, C. W. Chai and Y. S. Wu, *Mater. Chem. Phys.*, 105 (2007) 331.
10. H. H. Zhang, X. L. Pang, M. Zhou, C. Liu, L. Wei and K. W. Gao, *Appl. Surf. Sci.*, 356 (2015) 63.
11. F. G. Liu, M. Du, J. Zhang and M. Qiu, *Corros. Sci.*, 51 (2009) 102.
12. J. Baldenebro-Lopez, A. Baez-Castro, D. Glossman-Mitnik, H. Hopfl, A. Cruz-Enríquez, V. Miranda-Soto, M. Parra-Hake and J. Campos-Gaxiola, *J. Mol. Struct.*, 1130 (2017) 951.
13. W. Măntele and E. Deniz, *Spectrochim. Acta. A.*, 173 (2017) 965.
14. M. A. Gough and G. J. Langley, *Rapid Commun. Mass Spectrom.*, 13 (1999) 227.
15. L. Zeng, G. A. Zhang, X. P. Guo and C. W. Chai, *Corros. Sci.*, 90 (2015) 202.
16. H. Nahali, H. B. Mansour, L. Dhouibi and H. Idrissi, *Constr. Build. Mater.*, 141 (2017) 589.

17. C. Zhang and J. Zhao, *Corros. Sci.*, 126 (2017) 247.
18. B. Li, J. Mao, T. Nawa and T. Han, *Constr. Build. Mater.*, 147 (2017) 79.
19. P. E. Dim, R. S. Fletcher and S. P. Rigby, *Chem. Eng. Sci.*, 140 (2016) 291.
20. V. Pandarinathan, K. Lepkov´, S I. Bailey and R. Gubner, *J. Electrochem. Soc.*, 160 (2013) C432.
21. G. Gece and S. Bilgiç, *Corros. Sci.*, 51 (2009) 1876.
22. I.B. Obot and Z.M. Gasem, *Corros. Sci.*, 83 (2014) 359.
23. L. L. Liaoa, S. Moa, H. Q. Luoa, Y. J. Fengb, H. Y. Yinb and N. B. Li, *Corros. Sci.*, 124 (2017) 167.
24. Z. Y. Hu, Y. B. Meng, X. M. Ma, H. L. Zhu, J. Li, C. Li and D. L. Cao, *Corros. Sci.*, 112 (2016) 563.
25. B. Zhao and L. K. Zou, *Adv. Mater. Res.*, 710 (2013) 41.

© 2018 The Authors. Published by ESG (www.electrochemsci.org). This article is an open access article distributed under the terms and conditions of the Creative Commons Attribution license (<http://creativecommons.org/licenses/by/4.0/>).